Modelling Resistive Wall Modes in ITER with Self-Consistent Inclusion of Drift Kinetic Resonances

Yueqiang Liu[1], M.S.Chu[2], I.T. Chapman[1] and T.C. Hender[1]

[1] Euratom/UKAEA Fusion Association, Culham Science Centre, Abingdon, OX14 3DB, UK
[2] General Atomics, San Diego, California 92186, USA

E-mail contact of main author: yueqiang.liu@ukaea.org.uk

abstract. We investigate drift kinetic effects on the resistive wall mode (RWM) stability in ITER plasmas, due to the mode resonance with magnetic precession drifts and/or bounce motion of bulk plasma thermal particles. A toroidal drift kinetic model is self-consistently incorporated into the MHD formulation. Self-consistent simulations using the hybrid kinetic-MHD code MARS-K [Y.Q. Liu, *et al.*, Phys. Plasmas, in press (2008)] predict a parameter space for ITER steady state plasmas, where the RWM is fully stabilised by the drift kinetic effects combined with the toroidal plasma flow. A wider stable parameter space is predicted by the perturbative approach based on the ideal kink mode or the fluid RWM eigenfunction. The difference is attributed primarily to the self-consistent determination of the mode eigenvalue in the non-perturbative approach.

1 Introduction

Advanced tokamak scenarios, including those foreseen for ITER, aim at simultaneously maximising the plasma pressure and operating in steady state. This requires that all slowly evolving macroscopic MHD instabilities be stable. It is well known that the resistive wall mode (RWM), which is a global kink-like, non-axisymmetric instability, with growth rates reduced by the surrounding conducting wall(s), poses a limit to the steady state operation of advanced tokamaks. Therefore, it is critical to ensure that this mode stays stable when the plasma pressure exceeds the ideal no-wall beta limit.

Two approaches to stabilise the mode have been under extensive investigation during recent years, namely active control and rotational stabilisation of the mode, with kinetic damping effects being involved. The physics of rotational (or kinetic) stabilisation of the RWM remains unresolved, especially in view of the new experimental evidence from DIII-D [1, 2] and JT-60U [3], where balanced neutral beam injection produces RWM stable plasmas with very slow toroidal flow. Understanding the damping physics of the RWM is of significant importance not only for predicting the critical rotation speed to stabilise RWMs in ITER plasmas, but also for understanding other related physics effects, such as the resonant field amplification (RFA) [4], and plasma momentum damping (one of the momentum damping mechanisms, the neoclassical toroidal viscous damping, depends on RFA).

In this work, we apply a recently developed full toroidal drift kinetic model [5] to predict the RWM stability in ITER advanced scenarios [6]. This model is based on drift kinetic resonance damping of the mode at relatively low mode frequencies in the plasma frame [7, 8]. In contrast with Refs. [9, 10], we include the kinetic terms self-consistently in the MHD equations, which allows us to compute the kinetic energy perturbation using the RWM eigenfunction modified

by drift kinetic effects. In the perturbative approach, the kinetic energy is normally evaluated with eigenfunctions computed for an ideal kink mode. A significant feature of the new model, compared with our previous semi-kinetic model [11, 12, 13], is the full toroidal geometry in which we evaluate the kinetic integrals. One of the major purposes of this work is to compare the predictions for the RWM stability in ITER, following both perturbative and self-consistent approaches.

2 Kinetic formulation and benchmarking

While the self-consistent kinetic model is described in detail in [5], here we present a brief summary of the key elements of this formulation. We consider the single fluid MHD description of plasmas with a toroidal flow. The core equations, where the kinetic terms are involved, are written in the Eulerian frame

$$
\begin{aligned}
(\gamma + in\Omega)\xi &= \mathbf{v} + (\xi\cdot\nabla\Omega)R\hat{\phi}, && (1)\\
\rho(\gamma + in\Omega)\mathbf{v} &= -\nabla\cdot\mathbf{p} + \mathbf{j}\times\mathbf{B} + \mathbf{J}\times\mathbf{Q} - \rho\left[2\Omega\hat{\mathbf{Z}}\times\mathbf{v} + (\mathbf{v}\cdot\nabla\Omega)R\hat{\phi}\right], && (2)\\
(\gamma + in\Omega)\mathbf{Q} &= \nabla\times(\mathbf{v}\times\mathbf{B}) + (\mathbf{Q}\cdot\nabla\Omega)R\hat{\phi}, && (3)\\
(\gamma + in\Omega)p &= -\mathbf{v}\cdot\nabla P, && (4)\\
\mathbf{j} &= \nabla\times\mathbf{Q}, && (5)\\
\mathbf{p} &= p\mathbf{I} + p_{\parallel}\hat{\mathbf{b}}\hat{\mathbf{b}} + p_{\perp}(\mathbf{I} - \hat{\mathbf{b}}\hat{\mathbf{b}}), && (6)
\end{aligned}
$$

where the variables $\xi, \mathbf{v}, \mathbf{Q}, \mathbf{j}, \mathbf{p}$ represent the plasma displacement, perturbed velocity, magnetic field, current, and pressure tensor, respectively. ρ is the unperturbed plasma density, γ the eigenvalue, n the toroidal mode number, and Ω the plasma rotation frequency along the toroidal angle ϕ. The equilibrium field, current, and pressure are denoted by $\mathbf{B}, \mathbf{J}, \mathbf{P}$, respectively. R is the plasma major radius, $\hat{\mathbf{Z}}$ the unit vector in the vertical direction, $\mathbf{I}$ the unit tensor.

The kinetic terms enter the MHD equations via the perturbed kinetic pressure tensors shown in Eq. (6), where p is the scalar fluid pressure perturbation, and $p_{||}(\xi_{\perp}), p_{\perp}(\xi_{\perp})$ are the parallel and perpendicular components of the kinetic pressure perturbations respectively, and $\hat{\mathbf{b}} = \mathbf{B}/B, B = |\mathbf{B}|$. The full pressure tensor $\mathbf{p}$ is self-consistently fed back into the MHD formulation via equation (2).

The perturbed kinetic pressures are calculated from

$$
p_{\parallel}e^{-i\omega t + in\phi} = \sum_{e,i}\int d\Gamma M v_{\parallel}^2 f_L^1, \qquad p_{\perp}e^{-i\omega t + in\phi} = \sum_{e,i}\int d\Gamma \frac{1}{2} M v_{\perp}^2 f_L^1,
$$

where an $\exp(-i\omega t + in\phi)$-dependence is explicitly assumed for the perturbation, with the mode frequency $\omega \equiv i\gamma$. The integral is carried out over the particle velocity space Γ. M is the particle mass, $v_{\parallel}, v_{\perp}$ are the parallel and perpendicular (to the equilibrium magnetic field) velocity of particle local bounce motion, f_L^1 is the perturbed distribution function defined in the Lagrangian frame and calculated analytically following Refs. [7] and [8].

A derivation resulting in forms of $p_{||}$ and $p_{\perp}$, suitable for the numerical implementation, is presented in [5]. A key factor in the kinetic pressure terms is the mode-particle resonance

operator entering into f_L^1

$$\lambda_{ml} = \frac{n[\omega_{*N} + (\hat{\varepsilon}_k - 3/2)\omega_{*T} + \omega_E] - \omega}{n\omega_d + [\alpha(m+nq)+l]\omega_b - i\nu_{\text{eff}} - \omega}, \tag{7}$$

where ω_{*N} and ω_{*T} are the diamagnetic drift frequencies due to the density and temperature gradients, respectively, ω_E is the $\mathbf{E}\times\mathbf{B}$ plasma rotation, ω_b the particle transit/bounce frequency, ω_d the bounce-orbit-averaged toroidal precession drift frequency of particles, including the ω_E drift. $\hat{\varepsilon}_k = \varepsilon_k/T$ is the particle kinetic energy normalised by the temperature. ν_{eff} is the effective collisionality. $\alpha = 1$ for passing particles, and $\alpha = 0$ for trapped particles. m and l are the Fourier harmonic indexes over the poloidal angle and the particle bounce orbit, respectively. The latter implies projecting a time dependent periodic function, associated with the particle periodic bounce motion, on a basis function $\exp(il\omega_b t)$. We emphasise that the mode eigenvalue γ enters Eq. (7) non-linearly via $\omega \equiv i\gamma$. A special case of the kinetic resonance, valid at slow plasma rotation, comes from the toroidal precession of trapped ions or electrons. For this case, we set $\alpha = 0$ and $l = 0$ in Eq. (7).

Our self-consistent kinetic formulation neglects the perturbed electrostatic potential, the radial excursion of particle trajectory (finite banana width for trapped particles), as well as the FLR corrections to the particle orbit. These effects normally are not important for the RWM. Some of them are crucial to study the kinetic effects on other MHD modes, such as the internal kink mode. Although the formulation is presented for thermal particles, for which a Maxwellian distribution function over the particle energy is assumed, it is relatively easy to extend it to include, for instance, the fast ion contribution or an anisotropic distribution function.

Different from the self-consistent kinetic approach described above, a perturbative approach has been implemented in several codes for studying the kinetic effects on the RWM [9, 10]. In [10], the MHD stability code MISHKA [14] is coupled to the particle orbit-following code HAGIS [15] (Release Version 8.09). The perturbative approach normally uses the eigenfunction of the ideal kink mode, computed by an ideal MHD code, as the input to further compute the kinetic energy δW_k. The stability of the RWM is then determined by a dispersion relation derived from the kinetic MHD energy principle [16, 17]

$$\gamma\tau_w^* \simeq -\frac{\delta W_\infty + \delta W_k}{\delta W_b + \delta W_k}, \tag{8}$$

where δW_∞ and δW_b are the fluid potential energy without and with a conducting wall, respectively. The fluid energy includes both the plasma and the vacuum contributions. The normalisation factor τ_w^* is related to the wall eddy current decay time. In a cylindrical geometry, $\tau_w^* = \tau_w(1-b^{-2|m|})/|m|$, with b being the minor radius of the wall, and τ_w defined as the longest eddy current decay time of the wall.

The self-consistent approach differs from the perturbative approach in at least three aspects: (i) the kinetic modification of the eigenmode structure is taken into account; (ii) the eigenvalue of the kinetic RWM is self-consistently (and non-linearly) included in evaluating the kinetic integrals; (iii) in addition to the drift kinetic damping, the fluid continuum damping (due to the mode resonance with the Alfvén and sound waves) is also present in the self-consistent calculations.

Both perturbative and self-consistent approaches are realised in the kinetic-MHD code MARS-K [5].

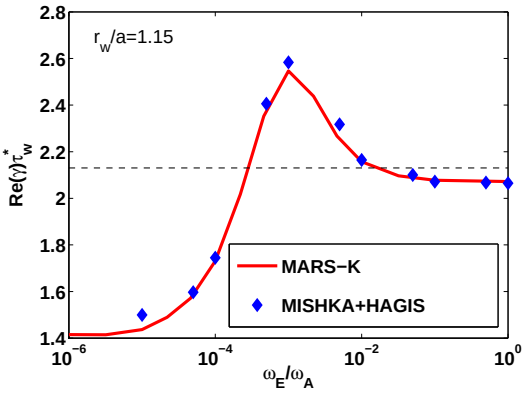

Figure 1: Comparison of the $n = 1$ RWM growth rates computed by MARS-K and HAGIS, following a perturbative inclusion of the precessional drift resonance damping from trapped thermal ions. A Solov'ev equilibrium is considered with aspect ratio of 5 and nearly circular poloidal plasma cross section. Uniform plasma density and rotation profiles are used.

Figure 1 shows an example of the growth rate comparison for the $n = 1$ kinetic RWM computed by MARS-K and HAGIS, following the perturbative approach. The no-wall ideal kink eigenfunction is used for computing the kinetic integrals. The magnetic precessional drift resonance of trapped thermal ions alone is included in the calculations by both codes. A test Solov'ev equilibrium, with aspect ratio of 5 and nearly circular poloidal plasma cross section, is considered. In addition, we assume a uniform radial profiles for the plasma equilibrium density and toroidal rotation ω_E. For the benchmark purpose only, we scan the rotation frequency ω_E from zero up to the Alfvén frequency, which is normally un-physical but covers the high frequency limit. We also neglect the mode frequency ($\omega = 0$) and the fluid effect of rotation on the ideal kink eigenfunction. The dashed horizontal line in the figure indicates the growth rate of the fluid RWM without kinetic effects and with no plasma rotation. Depending on the rotation speed, ion precession drift resonances alone can lead to either stabilisation or destabilisation of the RWM. Inclusion of the electron contribution, however, gives partial stabilisation of the mode for all rotation frequencies for this case. Good agreement between MARS-K and HAGIS is obtained. Equally good agreement is achieved under other assumptions (e.g. with both the ion and electron contributions) or for other equilibria [5].

Since the HAGIS code performs a full particle guiding centre orbit integration for the kinetic integrals, the agreement between two codes indicates that neglect of the particle banana width, an assumption made in the MARS-K formulation, is reasonable for such a low frequency mode as the RWM. We point out that, although the benchmark is made on the perturbative approach, it does test the major part of the self-consistent procedure, which relies on the same kinetic integrals as the perturbative approach.

3 Kinetic effects on RWM stability in ITER

We apply MARS-K to investigate the drift kinetic effects on the stability of the RWM for ITER steady state plasmas from Scenario-4 [6]. This scenario has a highly shaped plasma

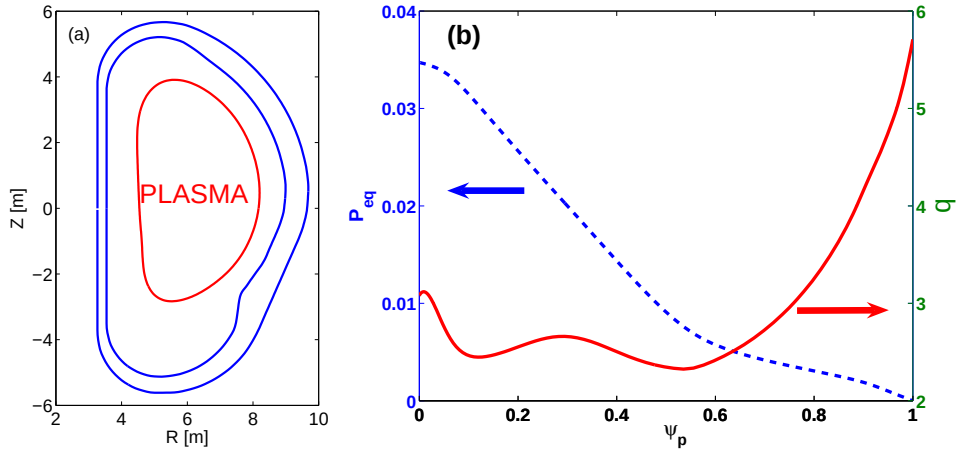

Figure 2: The ITER equilibrium adopted in this study. Shown are (a) the plasma boundary and the ITER double wall shape and (b) the equilibrium pressure, normalised by the magnetic pressure, and the safety factor profiles at $\beta_N = 3.0$. The plasma boundary shape is smoothed near the X-point of the lower single null configuration, for a sake of alleviating numerical difficulty.

with weak negative magnetic shear at the plasma core. The target plasma, which is marginally unstable to the $n = 1$ ideal external kink mode without a conducting wall, is designed to produce 340 MW fusion power at $Q = 5$. We scale the plasma pressure up to the ideal-wall (inner vacuum vessel) beta limit, while keeping the total plasma current at the design value of 9MA. For the sake of numerical accuracy, we smooth slightly the plasma boundary close to the X-point, without a significant modification of stability limits. The plasma boundary shape and the equilibrium pressure and safety factor profiles are shown in Fig. 2(a-b). Compared to the original equilibrium as reported in [12], the no-wall β_N limit is shifted from 2.45 to 2.33, and the ideal-wall limit from 3.65 to 3.62 by smoothing, according to MARS-F calculations. Following convention, we define an equilibrium pressure scaling factor $C_\beta \equiv (\beta_N - \beta_N^{\text{no-wall}})/(\beta_N^{\text{ideal-wall}} - \beta_N^{\text{no-wall}})$, so $C_\beta > 0$ corresponds to β_N above the no-wall limit. All the results reported in this Section are obtained for $C_\beta > 0$. The collisionality coefficient ν_{eff} is set to 0 for both ions and electrons throughout the ITER calculations presented below. This means we consider collisionless plasmas for both ions and electrons.

Figure 3 shows the fluid potential energy of the ideal kink mode (with or without a perfectly conducting wall with the ITER inner wall shape) versus C_β, together with the drift kinetic energy (both real and imaginary parts) computed by MARS-K following the perturbative approach. The perturbed kinetic potential energy (δW_k) comes from the precessional drift resonances of the RWM with trapped thermal ions and electrons (the effect of bounce resonances not being included in this calculation). All energies are normalised by the plasma inertia, computed using only the displacement perpendicular to the equilibrium magnetic surfaces, of the no-wall ideal kink mode. The ion and electron temperatures are taken equal, which is a reasonable assumption for ITER. The growth rate of the fluid RWM γ_f is used as the complex mode frequency $\omega = i\gamma_f$ in the kinetic integration. We keep the plasma rotation profile as predicted by the ASTRA simulation [6], but vary the rotation amplitude over a wide range. Figure 3 shows an example for a very slow plasma rotation, with the central rotation frequency at 10^{-3} of the Alfvén frequency. The precessional drift resonance is expected to provide the dominant

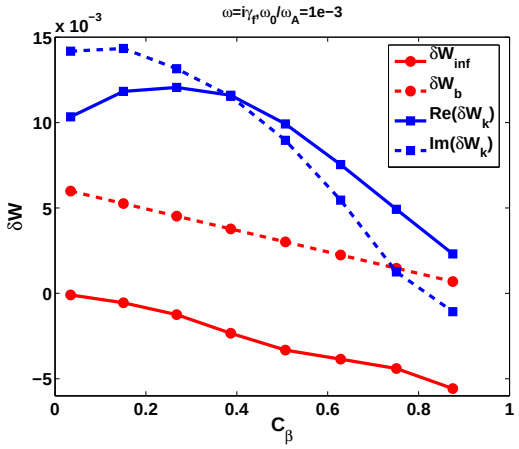

Figure 3: The energy perturbations computed by MARS-K, versus the equilibrium pressure scaling factor C_β for the ITER steady state plasma. Plotted are the fluid potential energy of the ideal kink mode, together with the perturbatively computed kinetic energy from precessional drift resonances of the RWM with trapped thermal particles.

damping at this rotation frequency. The eigenfunction of the no-wall ideal kink mode is used in evaluating the kinetic integrals. We notice a rather large and positive real part of the kinetic energy at relatively small C_β, indicating a strong cancellation of the negative (destabilising) fluid energy.

The fluid and kinetic energy perturbations shown in Fig.3 are used to estimate the growth rates of the kinetic RWM, following the dispersion relation (8). The results are shown in Fig.4. The perturbative approach predicts a full kinetic stabilisation of the RWM for a large range of C_β ($0 \leq C_\beta \lesssim 0.8$) at slow plasma rotation. We emphasise that the stabilisation comes solely from the mode resonance with the precession drifts of trapped particles.

For the ITER plasma with relatively slow toroidal rotation, addition of the kinetic contribution from the mode resonance with particle bounce motion does not modify significantly the pictures shown by Fig.3 and 4. As an example, figure 5(a) compares the MARS-K computed kinetic energy from precessional drift resonance alone, with that from both precessional and bounce resonances. The perturbative approach is followed for an ITER plasma with $C_\beta = 0.5$. The plasma central rotation frequency ω_0 varies from $2 \times 10^{-4}\omega_A$ to $2 \times 10^{-2}\omega_A$. Figure 5(b) compares the growth rate of the RWM under the same conditions. The contribution of the bounce resonance damping becomes visible only for the central rotation frequency ω_0 larger than $5 \times 10^{-3}\omega_A$. This contribution almost vanishes for $\omega_0 \lesssim 10^{-3}\omega_A$. The predicted plasma central rotation is less than $2\%\omega_A$ for ITER advanced Scenario-4 [6]. The predicted rotation frequency at the $q = 3$ surface is less than $0.25\%\omega_A$. (The $q = 2$ surface is absent for these ITER plasmas.) The calculation results show that, at the rotation speed predicted for ITER advanced plasmas, the particle bounce resonance damping plays a minor role. In the computations presented hereafter, we include only the precessional resonance damping from trapped particles. We also notice that the real part of the kinetic energy stays positive (i.e. stabilising) and increases with decreasing rotation frequency, leading to a strong mode suppression at very slow rotation.

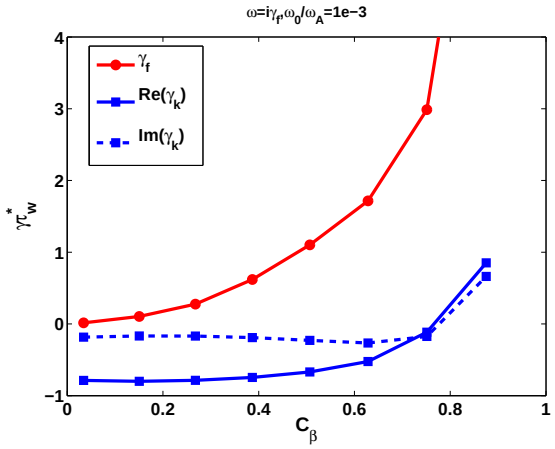

Figure 4: The growth rate of the RWM versus C_β, under the fluid description (γ_f) is compared with that of the kinetic RWM following the perturbative approach (γ_k). Both the growth/damping rate and the real frequency of the kinetic RWM are plotted, for the same ITER plasma as in Fig.2. γ_k is evaluated using formula (8).

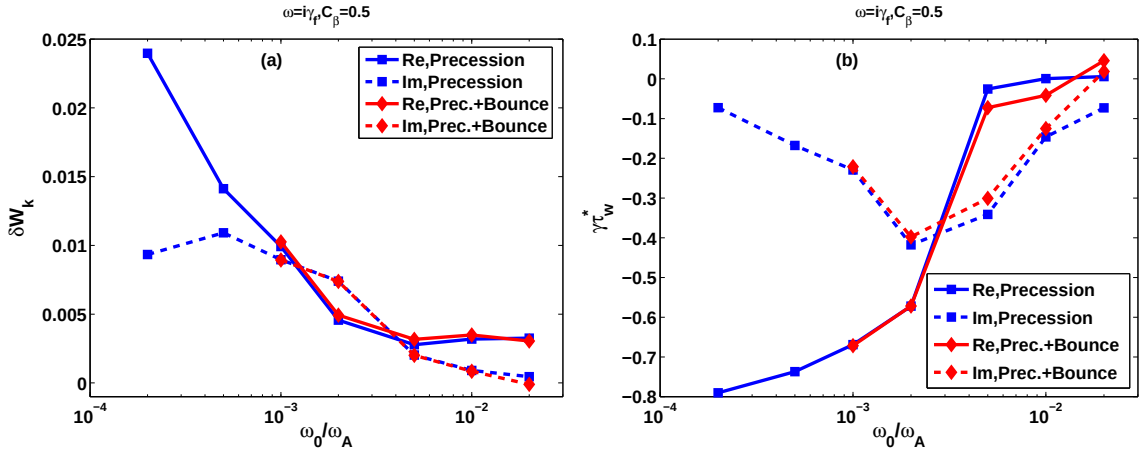

Figure 5: Comparison of (a) the kinetic energy perturbations and (b) the eigenvalue of the kinetic RWM, computed from precessional drift resonance alone, with that from both precessional and bounce resonances. The perturbative approach is followed for an ITER plasma with $C_\beta = 0.5$. The plasma central rotation frequency varies from $2 \times 10^{-4}\omega_A$ to $2 \times 10^{-2}\omega_A$.

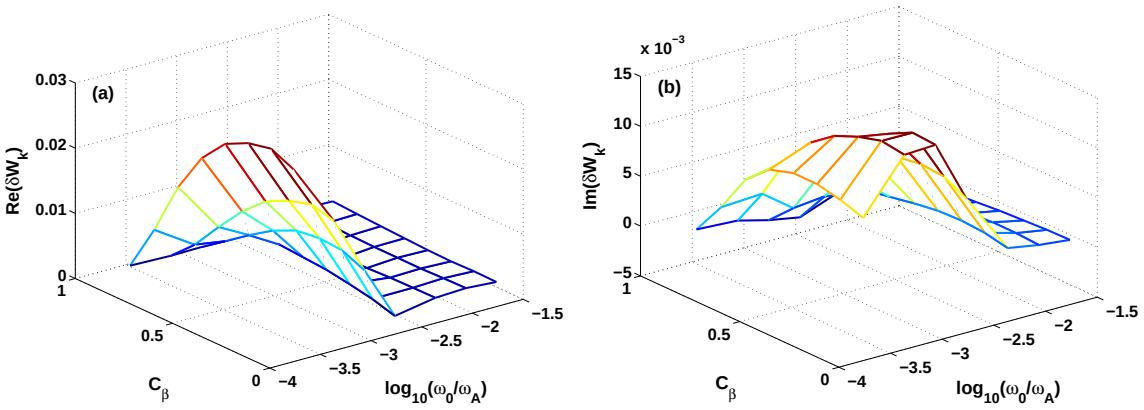

Figure 6: 2D plots of (a) real and (b) imaginary parts of the drift kinetic energy contribution for ITER advanced tokamak plasmas, predicted by the perturbative kinetic calculations using the no-wall ideal kink eigenfunction. Only precessional resonance damping is included.

Figures 6(a-b) show the variation of the computed drift kinetic energy in the parameter space of both plasma pressure and rotation speed. The pressure scaling parameter C_β varies between 0 and 0.9. The central rotation frequency ω_0 varies between $2\times10^{-4}\omega_A$ and $2\times10^{-2}\omega_A$. The perturbative approach is followed using the no-wall ideal kink eigenfunction. We notice that the imaginary (damping) part of the perturbed kinetic energy is comparable to that of the real (inertial) part. The most significant contribution is obtained near the corner of low C_β and slow rotation speed, indicating a large effect on the RWM growth rate in this corner. We also notice that the real part of δW_k does not vanish for the rotation speeds around $2\times10^{-2}\omega_A$.

Figures 7(a-b) plot the real and imaginary part of the RWM eigenvalues, by inserting the computed δW_k as shown in Fig. 6 into the dispersion relation (8). A full stabilisation of the mode, denoted by black dots in Fig. 7(a), is achieved in a wide range of parameter space (C_β, ω_0). For rotation frequencies below $3\times10^{-3}\omega_A$, full RWM suppression is obtained for C_β up to 0.8. Conversely, for C_β below 0.4, full stabilisation is obtained for rotation frequencies up to $2\times10^{-2}\omega_A$. In the remaining region, the RWM is not completely stabilised by the kinetic effects, but the growth rate is significantly reduced compared with that from the fluid prediction.

In the perturbative approach, it is expected that physically more accurate results are obtained by using the eigenfunction of a marginally stable, ideal-wall ideal kink mode [9], compared to that of the no-wall ideal kink. The former is normally closer to the true RWM eigenfunction in terms of the fluid resonant behaviour near rational surfaces. MARS-K, however, allows a direct use of the fluid RWM eigenfunction, which is probably the best approximation that one can expect in the perturbative approach. Using the fluid RWM eigenfunction, instead of the marginally stable ideal kink eigenfunction, allows numerical resolution of inertial layers, with the help of strong mesh packing for the radial grid near rational surfaces. This is because the width of the inertial layer, being proportional to the growth rate of the mode, is narrow but remains finite thanks to the finite growth rate of the fluid RWM.

We investigate the effect of inertial layer width on δW_k by varying the wall time from 0 (no-wall kink eigenfunction) to the true value of the ITER wall time (fluid RWM eigenfunction), which is about $6.2\times10^5\tau_A$. Figures 8(a-b) show the computed δW_k and the kinetic RWM

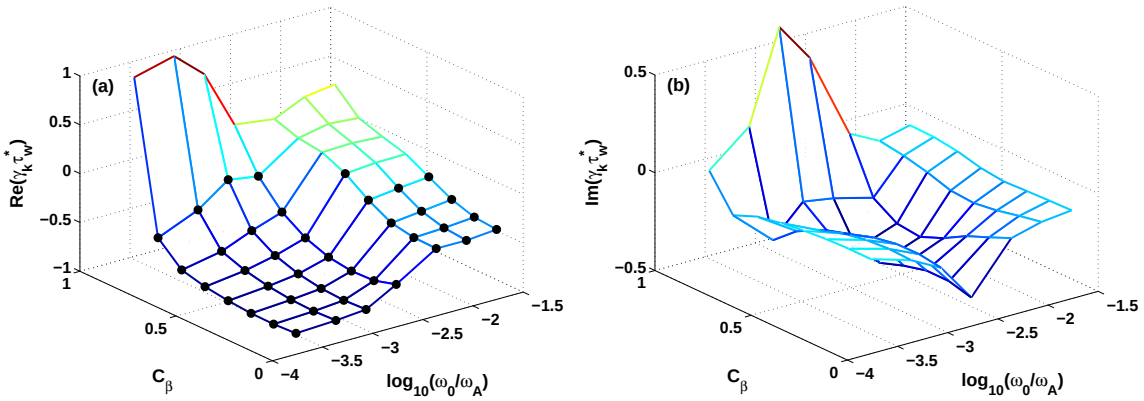

Figure 7: 2D plots of (a) real and (b) imaginary parts of the RWM eigenvalue for ITER advanced tokamak plasmas, predicted by the perturbative kinetic calculations using the no-wall ideal kink eigenfunction. Only precessional resonance damping is included. The black dots indicate stable RWMs.

eigenvalue respectively, versus τ_w. As the wall time increases, the growth rate of the mode decreases, and the width of the inertial layer near the rational surfaces decreases in proportion. The computed δW_k (both real and imaginary parts) also decreases but saturates well before the ITER wall time is reached. The reduction of δW_k is not significant for this ITER plasma. In fact, δW_k is reduced by about 15%, leading to a slight change of the kinetic RWM damping rate of about 10%. Note that the mode is still fully suppressed, as in the case with the no-wall kink eigenfunction.

Figure 9 shows the radial distribution of the computed drift kinetic energy for the above case with the true fluid RWM eigenfunction. The distribution is rather global across the whole plasma column. Non-negligible contribution also comes from the plasma edge. Another feature of this distribution is that no singularity is observed at the rational surfaces, despite the fact that the poloidal component of the RWM displacement, which enters the kinetic integrals, is normally rather singular near the rational surfaces. An exact cancellation of the singularity in the kinetic integrals for precessional drift resonances is expected from theory. This cancellation is numerically resolved in MARS-K computations by strong radial mesh packing near rational surfaces.

Figures 10 and 11 show 2D plots of the computed δW_k and the mode eigenvalues respectively, in the C_β - ω_0 plane using the fluid RWM eigenfunction in the perturbative approach. The drift kinetic energy is very similar to that using the no-wall ideal kink as shown in Fig. 6, and the region of stable kinetic RWM is also largely the same as that shown in Fig. 7.

Figures 12(a-b) show 2D plots of the kinetic RWM eigenvalue from self-consistent calculations. Compared with the perturbative results from Fig. 7 and 11, the region of full stabilisation is narrower according to the non-perturbative approach. The difference in the magnitude of eigenvalues between perturbative and non-perturbative approaches is due to differences in normalisation. In the former, the eigenvalue is estimated using the dispersion relation (8), where a normalisation factor τ_w^* is introduced. Strictly speaking, the perturbative approach using no-wall ideal kink eigenfunction does not assume any value for the wall time, because the wall resistivity is never involved in the calculations. The self-consistent approach does solve

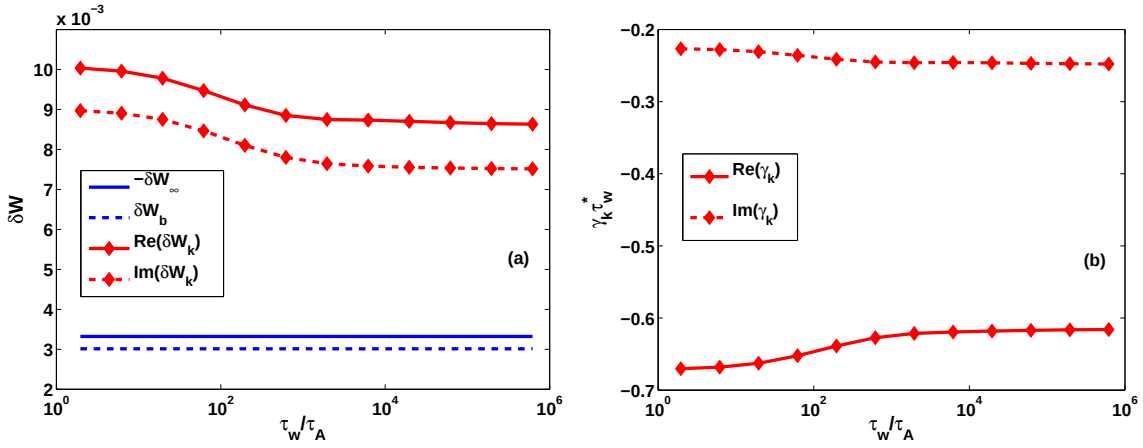

Figure 8: (a) The drift kinetic energy and (b) the kinetic eigenvalue versus the wall time for an ITER plasmas with with $C_\beta = 0.5$ and the plasma central rotation frequency at $10^{-3}\omega_A$. The perturbative approach is adopted with the fluid RWM eigenfunction and precessional resonances from trapped particles.

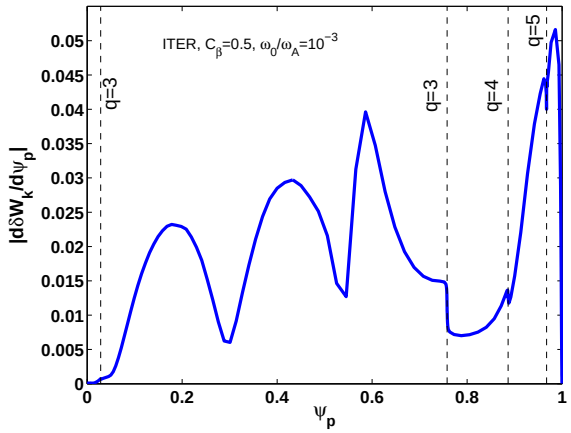

Figure 9: The kinetic energy density distribution from the perturbative approach using the fluid RWM eigenfunction.

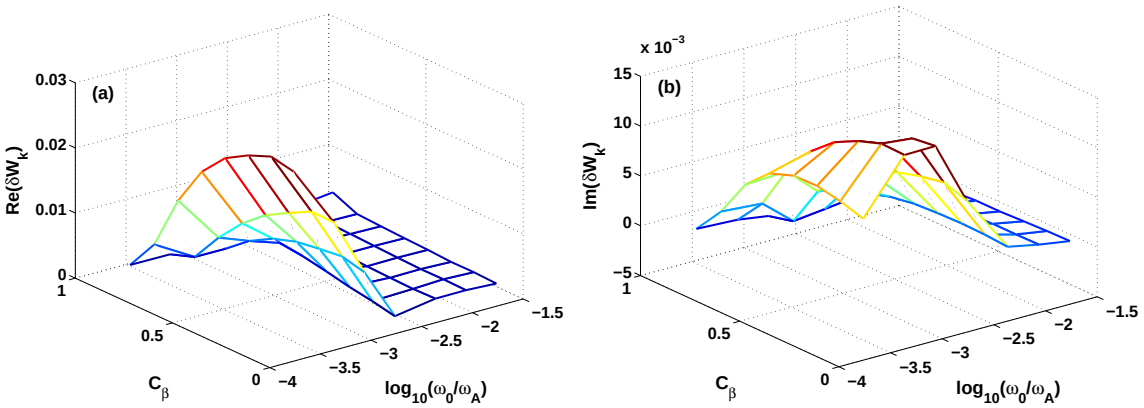

Figure 10: 2D plots of (a) real and (b) imaginary parts of the drift kinetic energy contribution for ITER advanced tokamak plasmas, predicted by the perturbative kinetic calculations using the fluid RWM eigenfunction. Only precessional resonance damping is included.

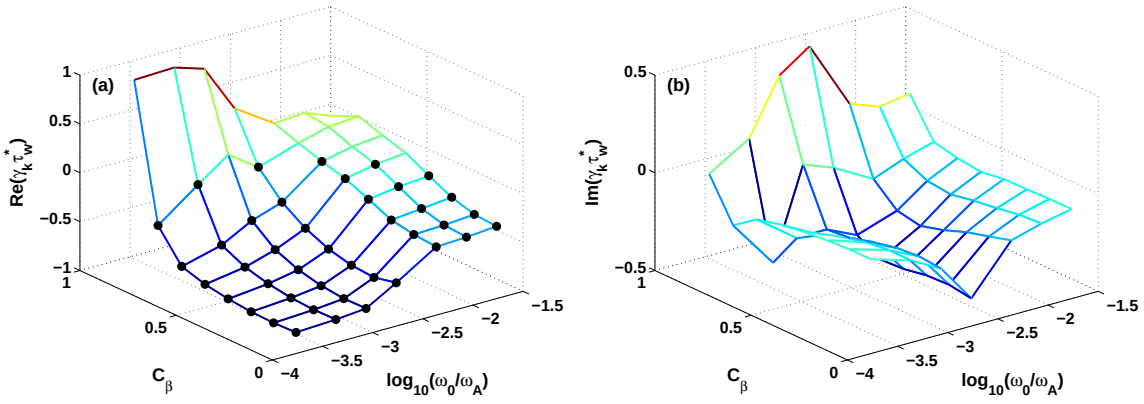

Figure 11: 2D plots of (a) real and (b) imaginary parts of the RWM eigenvalue for ITER advanced tokamak plasmas, predicted by the perturbative kinetic calculations using the fluid RWM eigenfunction. Only precessional resonance damping is included. The black dots indicate a stable RWM.

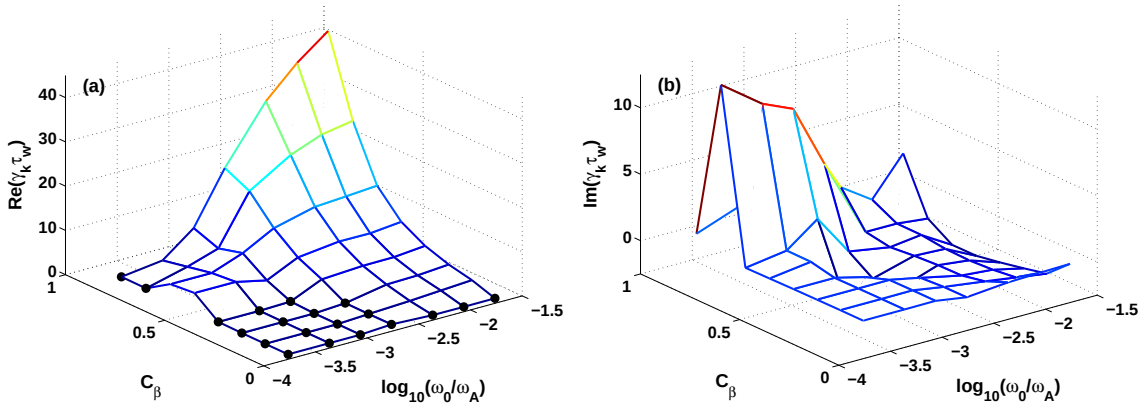

Figure 12: 2D plots of (a) real and (b) imaginary parts of the RWM eigenvalue for ITER advanced tokamak plasmas, predicted by the self-consistent kinetic calculations. Only precessional resonance damping is included. The black dots indicate stable RWMs with practically vanishing growth rates.

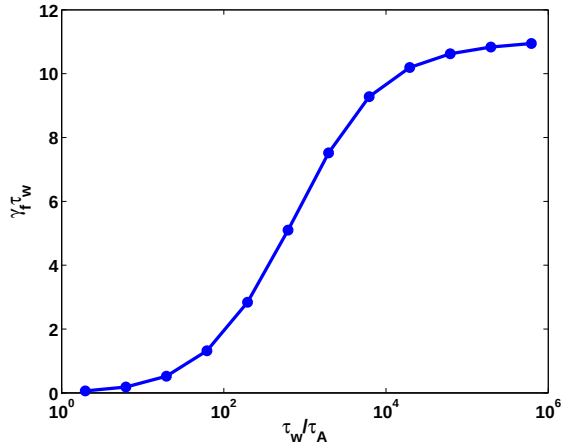

Figure 13: The growth rate of the fluid kink/RWM versus the wall time for an ITER plasma. The ITER double-wall time is about $6.2 \times 10^5 \tau_A$.

the MHD equations together with the eddy current equations for the resistive walls, hence the wall time τ_w is directly involved. At a large enough wall time (i.e. for very highly conducting walls), the plasma inertia becomes negligible, and the mode growth rate is mainly determined by the wall resistivity, hence the normalised growth rate $\gamma\tau_w$ is almost independent of τ_w. (In other words, the MARS-K computed γ is inversely proportional to τ_w.) As an example, for the ITER equilibrium with $C_\beta = 0.63$, the plasma inertia becomes negligible already at τ_w one order of magnitude below the true wall time, as shown by Fig. 13. Therefore, for the self-consistent calculations shown in Fig.12, we have chosen a wall time $\tau_w = 6.2 \times 10^4 \tau_A$, to avoid computing extremely small eigenvalues (in Alfvén units), and improve numerical accuracy. This brings a slight variation to the true growth rate of the kinetic RWM, without modifying the qualitative observations and conclusions.

In summary, both perturbative and self-consistent approaches predict a full stabilisation of the mode at low pressure ($C_\beta \lesssim 0.4$) and very slow toroidal rotation ($\omega_0/\omega_A \lesssim 2 \times 10^{-3}$), as indi-

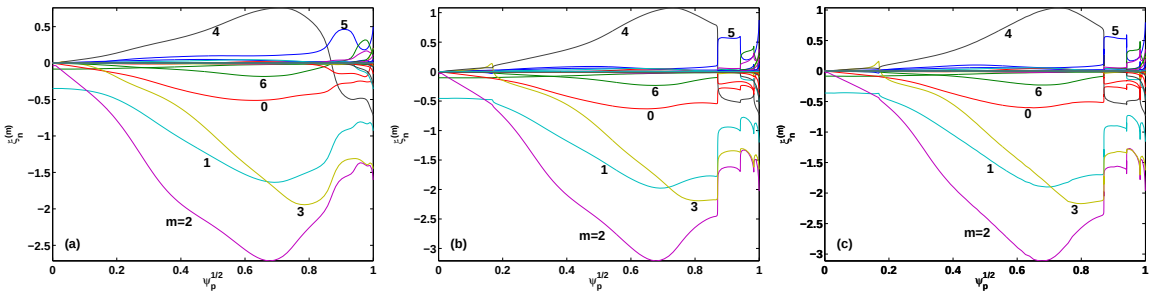

Figure 14: Comparison of the poloidal Fourier harmonics of eigenfunction (the radial displacement) for (a) ideal kink, (b) fluid RWM, and (c) kinetic RWM, computed by MARS-K for an ITER plasma with $C_\beta = 0.5$ and the plasma central rotation frequency at $10^{-3}\omega_A$. An equal-arc flux coordinate system is used in the numerical computations.

cated by the black dots in figures 7(a), 11(a) and 12(a). Using the fluid RWM eigenfunction, instead of an ideal kink in the perturbative calculations, gives very similar results. The perturbative kinetic approach predicts full stabilisation of the mode in a wider range of the $C_\beta - \omega_0$ domain. Similar observations have been made in both analytical calculations [18] and numerical tests for other plasma equilibria [5]. For a plasma close to the ideal-wall kink stability limit and with a rotation speed close to the predicted value for ITER, only partial stabilisation of the RWM is obtained by both approaches.

The difference in the predicted results between perturbative and non-perturbative approaches has been explained partially by the kinetic modification of the eigenmode structure, and partially by the nonlinear coupling of the RWM eigenvalue via the drift kinetic integrals [5]. Figures 14(a-c) compare the normal displacement computed for the no-wall ideal kink, the fluid RWM, and the self-consistent kinetic RWM. Whilst the no-wall kink eigenfunction is different from that of the fluid and kinetic RWM, especially near the rational surfaces, the latter two do not differ much. A careful examination of the perturbed kinetic pressures also does not reveal a significant difference between the fluid and the self-consistent kinetic RWM eigenfunctions. For ITER plasmas considered here, the difference in the stability prediction between the perturbative approach using the fluid RWM eigenfunction, and the self-consistent approach, is largely due to the nonlinear coupling of the mode eigenvalue in the kinetic integrals following the latter approach. This effect is also qualitatively demonstrated in an analytic model in Ref. [5].

4 Conclusions and discussions

A full toroidal drift kinetic damping model is self-consistently incorporated into the single fluid linear MHD formulation, via an anisotropic pressure tensor. This approach allows a self-consistent modification of the eigenmode structure and eigenvalue due to kinetic effects. Within the approximations made in this model, it provides a useful tool to study the damping physics of the unstable RWM, as well as the dynamics of a stable RWM.

For ITER steady state advanced scenarios, the self-consistent kinetic model predicts a full

stabilisation of the RWM at very slow plasma rotation (less than 0.2% of the Alfvén speed at the plasma centre) and moderately high plasma pressures ($C_\beta \lesssim 0.4$). More optimistic results are obtained by the perturbative approach, where the eigenfunction of ideal kink mode or the fluid RWM is used to evaluate the kinetic integrals, and an approximate dispersion relation is applied *a-posteriori* for estimating the mode eigenvalue. For the ITER plasmas, using the fluid RWM eigenfunction does not yield a significant difference for the stability of the kinetic RWM, compared with that using the no-wall ideal kink mode in perturbative calculations. The difference in the results between the perturbative and non-perturbative calculations is partially due to the modification of the RWM eigenfunction, but primarily due to the self-consistent determination of the mode eigenvalue in the latter approach. For a plasma toroidal rotation speed up to the predicted value for ITER, the kinetic damping of the RWM is mainly provided by precessional drift resonances of trapped thermal particles.

A similar conclusion of partial stabilisation is reached in [9] for an ITER like plasma, where marginally stable ideal kink mode eigenfunctions are used in the perturbative calculations. Recent perturbative kinetic simulations for JET plasmas [10] and self-consistent kinetic computations for DIII-D plasmas [19] also confirm the partial stabilisation of the RWM with drift kinetic effects. However, recent experimental results in DIII-D [20] seem to suggest a complete stabilisation of the RWM in the linear regime and in the absence of error fields. The latter two conditions, meaning the absence of the RWM coupling to other modes and to the magnetic braking, are assumptions implicitly made in all the above mentioned numerical calculations. In the presence of low level error fields, experiments do observe a finite, but very small critical rotation speed at about $0.3\%\omega_A$ at the $q = 2$ surface [1, 2]. The present kinetic theory offers a close, but not full explanation of these experimental observations, indicating the need to explore other damping mechanisms before giving a full account of ITER RWM stability.

In this work, we did not include the kinetic contribution from fast particles. The effect of the plasma collisionality is neglected. For ITER plasmas, it is probably important to consider the effect of electron collisions. A comprehensive prediction of the RWM stability in ITER may require including all these effects, as well as considering additional damping physics, such as the one derived from the nonlinear reactive closure in the advanced fluid theory [21]. We are also currently investigating the effect of background turbulence induced damping on RWM stability.

Acknowledgements

This work was funded by the United Kingdom Engineering and Physical Sciences Research Council and by the European Communities under the contract of Association between EURATOM and UKAEA. The views and opinions expressed herein do not necessarily reflect those of the European Commission. Work also supported by the US Department of Energy under DE-FG03-956ER54309.

We acknowledge many fruitful discussions with Dr. C.G. Gimblett and Dr. R.J. Hastie from UKAEA Culham on the kinetic effects. We also acknowledge very helpful communications with Prof. R. Betti concerning the drift kinetic energy distribution.

References

[1] H. Reimerdes, *et al.*, Phys. Rev. Lett. **98**, 055001 (2007).

[2] E.J. Strait, *et al.*, Phys. Plasmas **14**, 056101 (2007).

[3] M. Takechi, *et al. (JT-60 Team)*, Phys. Rev. Lett. **98**, 055002 (2007).

[4] A.H. Boozer, Phys. Rev. Lett. **86**, 5059 (2001).

[5] Yueqiang Liu, *et al.*, "Toroidal self-consistent modelling of drift kinetic effects on the resistive wall mode", Phys. Plasmas, in press (2008).

[6] Polevoi A. *et al.*, Fusion Energy 2002 (Proc. 19th Int. Conf. Lyon, 2002) (Vienna: IAEA) CD-ROM file CT/P-08 and http://www.iaea.org/programmes/ripc/physics/fec2002/html/fec2002.htm

[7] T.M. Antonsen and Y.C. Lee, Phys. Fluids **25**, 132 (1982).

[8] F. Porcelli, *et al.*, Phys. Plasmas **1**, 470 (1994).

[9] B. Hu, R. Betti, and J. Manickam, Phys. Plasmas **12**, 057301 (2005).

[10] I.T. Chapman, *et al.*, "Kinetic Effects on the Resistive Wall Mode", Plasma Phys. Control. Fusion, submitted (2008).

[11] A. Bondeson and M.S. Chu, Phys. Plasmas **3**, 3013 (1996).

[12] Yueqiang Liu, *et al.*, Nucl. Fusion **44**, 232 (2004).

[13] Y.Q. Liu, *et al.*, Nucl. Fusion **45**, 1131 (2005).

[14] A.B. Mikhailovskii, *et al.*, Plasma Phys. Rep. **23**, 844 (1997).

[15] S.D. Pinches, *et al.*, Comput. Phys. Commun. **111**, 133 (1998).

[16] S.W. Haney and J.P. Freidberg, Phys. Fluids B **1**, 1637 (1989).

[17] M.S. Chu, *et al.*, Phys. Plasmas **2**, 2236 (1995).

[18] Yueqiang Liu, *et al.*, Phys. Plasmas 15, 092505 (2008).

[19] Yueqiang Liu, *et al.*, BI2, Invited talk at 50th APS-DPP Annual Meeting, November 17-21, 2008, Dallas, Texas, to be submitted to Phys. Plasmas.

[20] E.J. Strait, *et al*, "DIII-D research in support of ITER", Fusion Energy 2008 (Proc. 22th Int. Conf. Geneva, 2008) (Vienna: IAEA) CD-ROM file OV/1-4.

[21] J. Weiland, private communications (2007).